

A machine vision system for tool wear assessment

S. Kurada and C. Bradley

Automated tool condition monitoring is gaining considerable importance in the manufacturing industry. This can be attributed to the transformation of manufacturing systems from manually operated production machines to highly automated machining centres. Modern image processing techniques and machine vision systems can now enable direct tool wear measurement to be accomplished in-cycle. Such a system, characterized by its measurement flexibility, high spatial resolution and good accuracy, is presented here. The system consists of a fibre-optic light source to illuminate the tool and a CCD camera (used in conjunction with a high resolution video zoom microscope) to capture the reflected pattern. The extent of the flank wear land has been determined using both textural and gradient operators; a texture operator has been implemented in the final system.

© 1997 Elsevier Science Ltd. All rights reserved

Keywords: *tool wear, machine vision, image processing, texture*

Introduction

The development of a reliable cutting tool monitoring system is an important step for the development of unmanned, computer numerically controlled (CNC) turning centres. In the absence of a human operator, the automated machining system must compensate for the lack of the human's experience and judgement abilities. Timely change of the cutting tool toward the end of its useful life prevents inferior surface finish quality (leading to scrap and re-work costs) or worse, damage to the machine tool itself. To achieve full automation at the machining centre, sensor technology is being adopted, in conjunction with associated decision making software, to gather pertinent data from the machine tool and decide on what control action should be taken. In the research literature, many single and multi-sensor strategies are being explored for reliable tool wear monitoring. Corresponding investigations into signal processing, sensor fusion, and artificial intelligence techniques are also being undertaken.

There are two predominant wear mechanisms that limit a tool's useful life: flank wear and crater wear. Flank wear occurs on the relief face of the tool and is mainly attributed to the rubbing action of the tool on the

machined surface. Crater wear occurs on the rake face of the tool and changes the chip–tool interface, thus affecting the cutting process. Tool wear increases progressively during machining dependent on the type of tool, material, cutting conditions, and lubricant selected. Traditionally, wear has been measured with a toolmaker's microscope under laboratory conditions. This requires a human inspector to determine the worn region based on the textural difference between the worn and the unworn surfaces. Flank wear is determined by measuring the maximum distance (termed $V_{B\max}$) between the top of the tool edge and the bottom of the worn surface¹. The complex nature of the tool wear complicates the task of defining the flank and crater wear boundaries manually. Obviously, the process is not in-situ and is time consuming.

A variety of experimental sensing techniques have recently been applied to the automated tool wear monitoring problem². The particular sensor method employed can be described as performing either a direct or indirect measurement. For example, a direct method of tool wear measurement employs a machine vision system to gauge the extent of the flank or crater wear, essentially emulating the role of the human inspector armed with the toolmaker's microscope³. The research described in this paper is under the direct measurement category.

Indirect sensing methods have predominantly been implemented, employing such varied technologies as

Department of Mechanical Engineering, University of Victoria, Victoria, BC, Canada V8W 3P6

Received for publication 10 August 1995; revised 20 February 1996; accepted 5 August 1996

acoustic emission, cutting force, spindle current, and vibration sensors. Acoustic emission (AE) sensors⁴ have been extensively researched because the sensor technology is readily available and the sensors are conveniently mounted on the lathe's tool holder. Unfortunately, much ancillary electronic hardware is required to preamplify, amplify, and filter the signals obtained. For example, lowpass filtering is necessary to remove high-frequency components of the sensor signal associated with chip breakage at the tool workpiece interface. AE sensors do generate a signal at a frequency much higher than the typical machine tool vibrations present but one must still isolate a representative tool wear signal and correlate it with tool wear. Alteration of the machine tool cutting conditions (feedrate, material, tool, etc.) could alter this relationship between signal and wear. Force sensing⁵ has also been extensively examined and requires the tool holder to be equipped with a transducer to measure the cutting forces along three orthogonal axes. This sensing technique is dependent on the dynamic and static stiffness properties of the particular machine under examination. Furthermore, tool wear creates only a small change in the cutting force, whereas changes in the cutting conditions generate large changes in the monitored force. Spindle current monitors are incorporated in many new machine tools but tend to be less sensitive than required for small depths of cut. Vibration sensing has shown some promise as a means of correlating machine tool vibration with tool wear^{6,7}. The vibrations arise from the shearing action of the tool and can be detected at the machine base by an accelerometer. Unfortunately, some expertise is required to select suitable regions of the vibration spectra which are related to the tool wear state. Most of these indirect techniques have shown some promise in the laboratory although industrial successes have been few.

By adopting techniques from the artificial intelligence community and employing multiple sensors, some of the problems described above have been minimized. Rangwala and Dornfeld⁸ applied neural network techniques to the multi-sensor tool wear monitoring problem. Neural networks allow an automatic learning capability so that some of the machine dependency problems could be eliminated. Neural networks also permit data from multiple sensors to be combined in order to use the maximum amount of information in a control decision. As more sensor-based data is utilized, the certainty of the derived tool wear parameters increases. In a similar manner, fuzzy systems have also been applied to the multi-sensor monitoring problem⁹.

Advances in computer vision technology have led to the investigation of its application in tool wear measurement. For example, Weis *et al.*¹⁰ have recently employed machine vision for monitoring milling and have measured the condition of inserts on an end mill during the machining process. However, for monitoring machining on a lathe, previous machine vision research has examined either the direct optical measurement of tool shape or the measurement of the tool's worn region. Vision systems have the inherent advantage of a direct (albeit intermittent) measurement of the tool wear. Some research has pursued the measurement of only flank wear, whereas others have attempted to

measure both flank and crater wear. Flank wear regions can be imaged with a camera; however, crater wear determination requires the projection of a structured light pattern onto the tool. The deformation of the structured pattern (typically parallel lines of laser light) is indicative of the depth of the crater on the tool's relief face. In this research work, only flank wear will be assessed as it is generally regarded as being the more important wear parameter and the one traditionally measured.

The majority of previous research on vision systems and flank wear have employed a simplistic image processing technique that is prone to generate erroneous results and performs unsatisfactorily in the presence of slightly changing illumination conditions or surface textures. Various researchers have employed the same fundamental image segmentation approach of histogram-based global thresholding of the image¹¹⁻¹³. Direct global thresholding delineates the two regions (worn and unworn) prior to deriving the morphological parameters that quantify the tool wear. Park and Ulsoy¹⁴ stated that successful segmentation of the image is key to obtaining satisfactory measurement of flank wear. Jeon and Kim¹⁵ tried illuminating the tool's wear zone with a laser beam but still encountered segmentation problems associated with surface irregularities. Hence, a more robust image analysis approach is required to process the grey scale images. A technique proposed here is to employ image segmentation based on the textural differences between the worn and unworn regions. The objective of this research is to develop a robust vision-based flank wear monitor, which could be successfully applied in an automated production environment, that improves upon the previous attempts at flank wear measurement.

Most of the existing vision-based monitors do not meet the above objective and their use is, therefore, limited to the laboratory environment. In this work, high resolution grey level images of the tool wear pattern are obtained with a CCD camera, connected to a video zoom microscope (VZM), used in conjunction with a fibre optic illumination source. Gradient and texture-based operators have been evaluated, and the results obtained from the vision system are compared with those obtained from the toolmaker's microscope.

Measurement system

A schematic diagram of the tool wear measurement system is shown in Fig. 1. In order to obtain adequate contrast between the worn and unworn tool regions, the intensity and angle of illumination of two fibre-optic guides were adjusted to accentuate the tool region of interest. A CCD camera, with a pixel resolution of 768×493 , was used in conjunction with the VZM and a frame grabber having an intensity resolution of 8 bits for analogue-to-digital conversion. The entire image analysis, starting with the digitized intensity matrix and ending in a set of tool wear parameters, was performed on a microcomputer (486 DX-66).

During monitoring, the tool is positioned such that the camera can focus on its flank face and a typical image of the tool's clearance face obtained is shown in Fig.

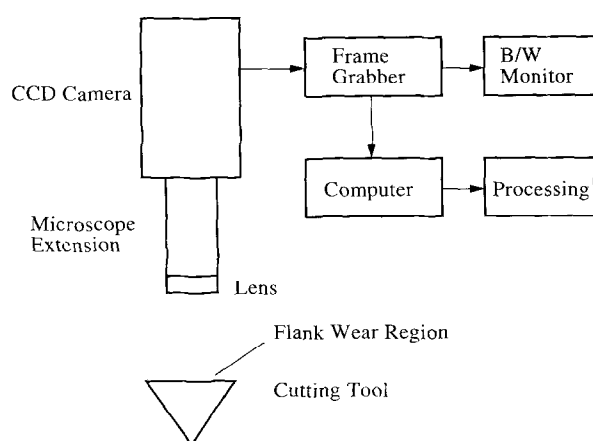


Fig. 1 Schematic diagram of the tool wear measurement system

2. The intensity variation of the light reflected from the surface is due to the textural variations between the distinct regions present. The magnified image of the cutting tool clearly shows three textural regions: (i) a wear region, characterized by a uniform texture, (ii) a background and (iii) an unworn region distinguished by a coarser texture than either the background or worn region.

To determine the wear parameters in SI units, the vision system was calibrated to determine suitable conversion factors. A set of parallel lines with known distances between them were focused under the microscope and their distance was measured in terms of pixels. The following factors were obtained:

Horizontal factor: $2.734 \mu\text{m}/\text{pixel}$
 Vertical factor: $2.812 \mu\text{m}/\text{pixel}$

These calibration factors were used to compute various flank wear parameters in terms of SI units.

Image processing

The functions of the image processing modules, as illustrated in Fig. 3, are to isolate and measure the wear region in an automated manner.

Image enhancement

As is evident in Fig. 2, the acquired image is corrupted by image noise; that is, random bright spots occurring in the image due to specular reflections off asperities on the tool surface. Positioning of the fibre optic illumination sources relative to the tool can minimize this effect; however, it cannot be totally eliminated. Therefore, the image is enhanced prior to the application of the segmentation operators by the application of a filter mask. Initially, a linear smoothing filter was applied to remove these high-frequency components; however, much of the important edge detail (between worn and unworn regions) was lost. A more successful image enhancement was achieved by applying a cascaded median filter (5×5 window) which preserves edge detail in the original image.

Image segmentation

The next block in the flowchart of Fig. 3 is the segmentation function necessary to extract the wear region pixels from the remainder of the image, which

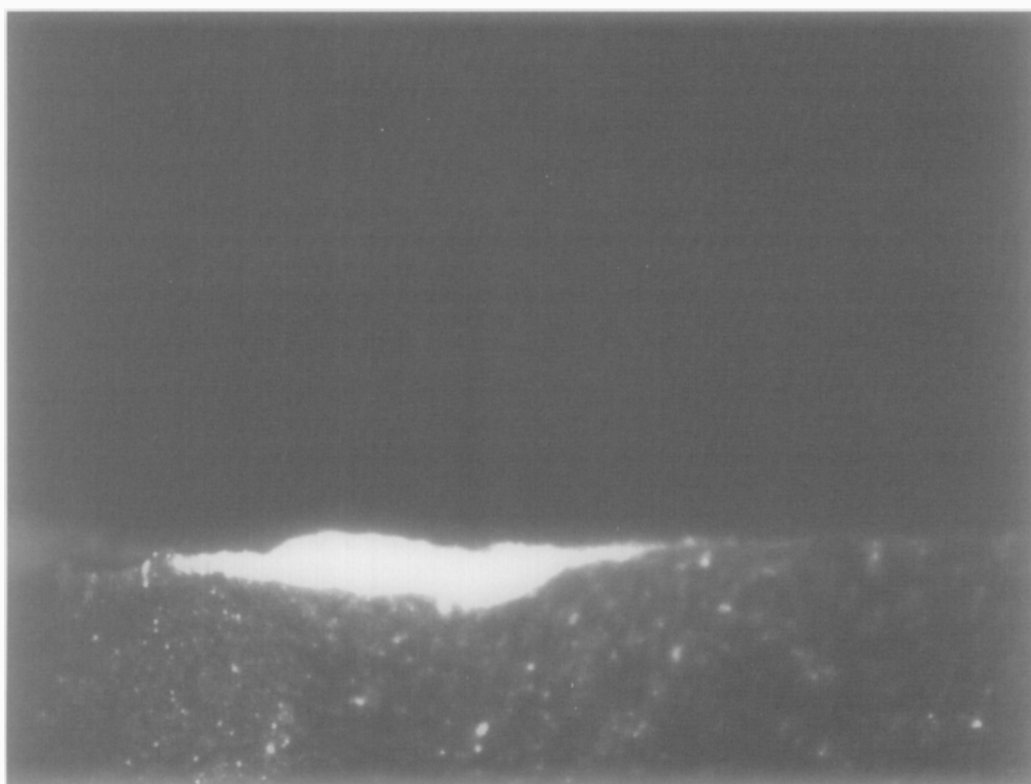


Fig. 2 Typical image of the cutting tool's clearance face

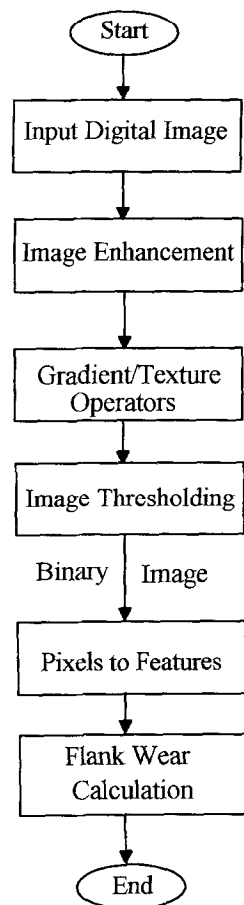


Fig. 3 Flowchart of the various steps involved in processing tool wear images

is composed of the background and the unworn tool region. Several operators have been evaluated in order to determine the most appropriate one for performing the tool image segmentation. Worn tool region segmentation has been evaluated through both edge operators (that directly define the worn region boundary) and texture operators (that find regions of similar surface texture).

An edge is a significant change in the local image intensity between, for example, the dark image background and the brighter region defining an object surface. By locating the image pixels that are edges in an image, and linking them together, the boundaries of objects can be defined. As the gradient of a function is a measure of change, edge detectors utilize gradient techniques to locate the edge pixels. Texture-based operators, however, rely on grouping pixels together based on some measure of similarity in texture within a region. Texture is the spatial distribution of grey levels in a local region. In segmentation through texture, a single homogeneous region is defined using grey level properties inherent to that region.

Edge operators

The magnitude of the two-dimensional gradient vector is approximately given by:

$$\left| \vec{G}[f(x,y)] \right| = \left| \begin{bmatrix} G_x \\ G_y \end{bmatrix} \right| \approx |G_x| + |G_y| \quad (1)$$

For digital imagery a discrete approximation to the gradient is used. The approximation to the derivatives uses the differences between neighbouring pixels calculated in a small local window. G_x and G_y are computed from the expressions:

$$G_x = (x_6) - (x_4) \quad G_y = (x_8) - (x_2) \quad (2)$$

where x_1, \dots, x_9 are the pixels in the underlying image. Two practical implementations of this concept are the Sobel and Frei-Chen operators. Both operators approximate G_x and G_y in a larger 3×3 window in order to minimize noise sensitivity. The kernels are shown in Table 1.

Sobel's operator weights the central row and column more heavily in computing G_x and G_y . The Frei-Chen operator employs a vector formulation for the detection of points, lines and edges, to detect any combination of these features¹⁶. The algorithm applies a set of 3×3 kernels to each image pixel and each kernel extracts a different feature in the image. The presence of an edge is obtained by applying the kernels in Table 1 to the input image. The resulting image from the application of the Frei-Chen operator, for example, is shown in Fig. 4(a).

Texture operators

Texture operators have received much attention in the image processing literature for their ability to perform superior segmentation in certain applications. Texture operators transform pixels with similar texture into pixels that have a similar brightness, thereby allowing segmentation to be completed by applying a simple brightness thresholding operation. The Hurst and variance texture operators are examined in this work.

The Hurst operator evaluates the texture of the surface brightness images through examination of the 2-D brightness variation in a circular window around each pixel¹⁷. The brightness variation is used to convert each original image pixel to a new brightness scale that is indicative of local surface roughness. Figure 5

Table 1 Sobel and Frei-Chen operators

Sobel	
$\begin{bmatrix} -1 & 0 & 1 \\ -2 & 0 & 2 \\ -1 & 0 & 1 \end{bmatrix}$	$\begin{bmatrix} 1 & 2 & 1 \\ 0 & 0 & 0 \\ -1 & -2 & -1 \end{bmatrix}$
Frei-Chen	
$\begin{bmatrix} 1 & 0 & -1 \\ \sqrt{2} & 0 & -\sqrt{2} \\ 1 & 0 & -1 \end{bmatrix}$	$\begin{bmatrix} -1 & -\sqrt{2} & -1 \\ 0 & 0 & 0 \\ 1 & \sqrt{2} & 1 \end{bmatrix}$

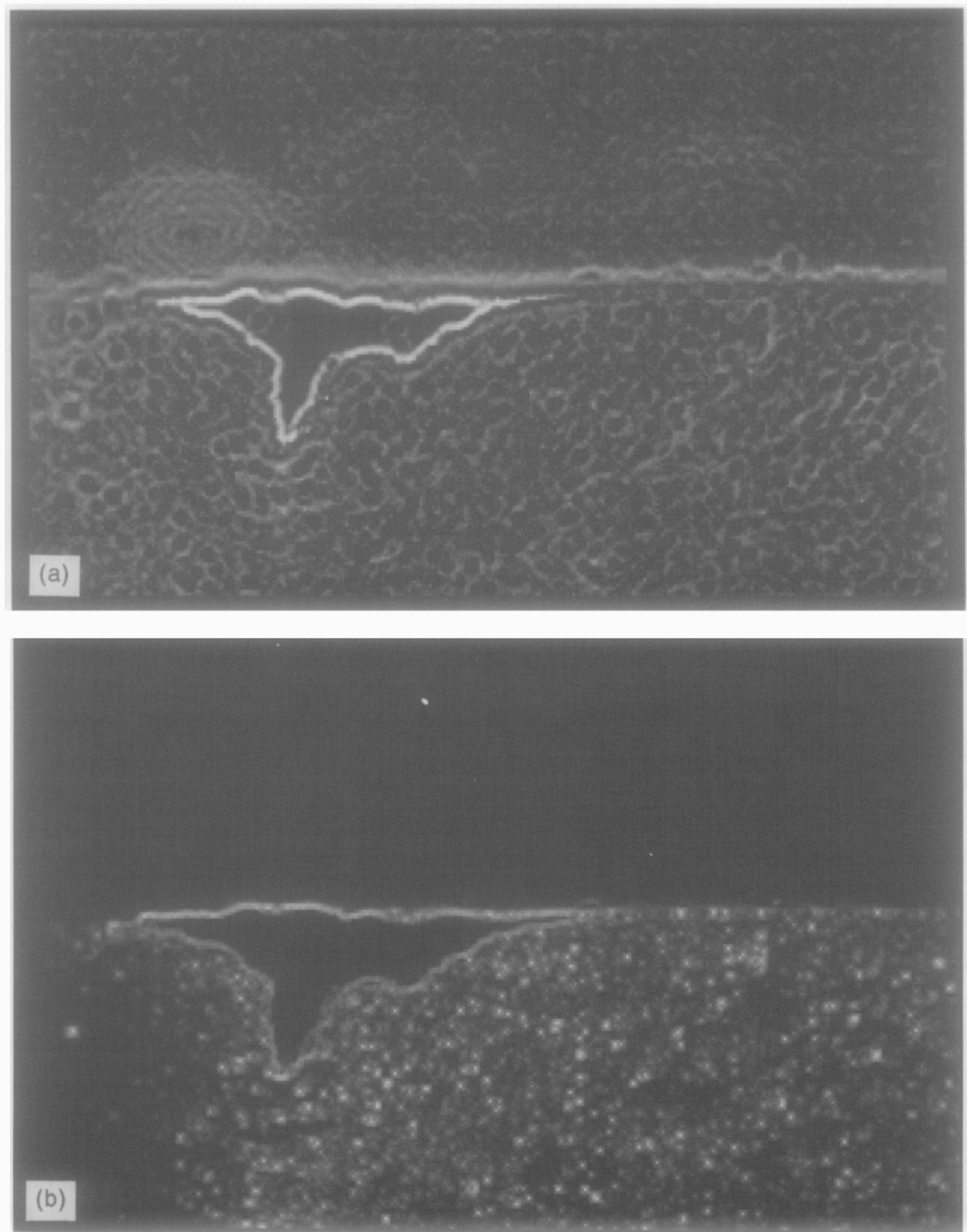


Fig. 4 Image obtained after applying: (a) the Frei-Chen operator; (b) the variance operator

shows a neighbourhood region consisting of 37 pixels in a 7-pixel wide octagonal shape. Each of the pixels in the diagram is labelled to indicate its distance from the centre of the octagon. For example, the immediate four neighbours ('b' pixels) have a distance of 1, whereas the most distant pixel is at $\sqrt{17}$. For each image pixel, a plot of \log (maximum brightness

difference) – \log (radial distance from operator centre) is constructed. The slope of the line is calculated from this plot by a least squares fit; the slope being directly related to the Hurst coefficient. The transformed brightness levels are now comparatively homogeneous within the worn region and segmentation can be accomplished through thresholding of the new brightness image.

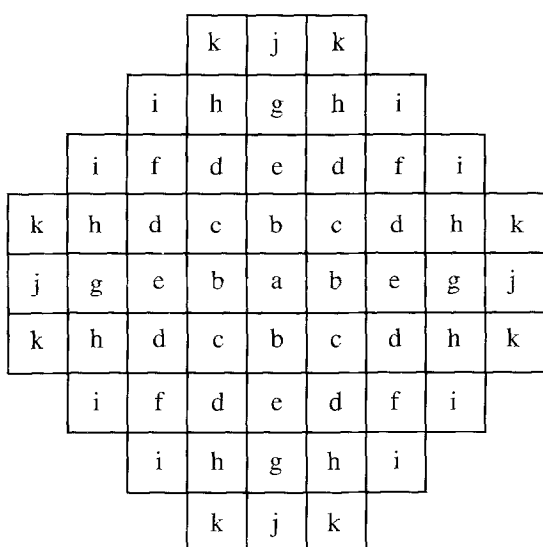


Fig. 5 Octagonal shaped neighbourhood region used in the Hurst operator

Variance in neighbourhood regions is another estimator of texture¹⁸. The original image is converted to one in which brightness represents the texture, and the operator responds well to the boundaries between regions of different brightness. The variance of the brightness values in a 5×5 mask around the pixel of interest is computed as the sum of the squares of the differences between the brightness of the central pixel and its neighbours. As the value of variance can be quite large, the square root of the value is used. Figure 4(b) illustrates the resulting image after application of the variance operator.

Selection of a segmentation operator

The investigation undertaken during the project revealed that the best segmentation performance is achieved by employing the variance operator. As is illustrated in Fig. 4(a), edge operators produce an output with poor discrimination along the boundary between worn and unworn regions. Furthermore, unwanted edges between light and dark regions within the worn region are also discernible. These erroneous edges around small irregular regions, internal to the wear land, generated further complexity in the downstream image processing. To circumvent these additional complexities, texture-based segmentation employing the variance operator has been selected. The Hurst operator appears to perform more effectively when the image has textures present across a broader scale of resolutions.

The resulting brightness image (post segmentation) is converted to a binary image by automatic selection of an optimum threshold value from the histogram. The variance operator generates an image in which the brightness values are homogeneous within the three regions. If the original tool image, as shown in Fig. 2, had simply been globally thresholded, the bright areas present on the tool's un-worn region would also be assigned a high value or 1 in the binary image. In contrast, however, the image resulting from the vari-

ance operator, shown in Fig. 4(b), has a much improved definition of the worn region.

Pixels to features

It is necessary to isolate the pixels, which have been collected within the wear region boundary, into an identifiable morphological feature from which a set of useful tool wear parameters can be calculated. The initial processing step is to identify clusters of connected non-zero valued pixels, described as blobs, in the binary image. The algorithm proceeds from top to bottom, scanning left to right, and collects bright pixel run lengths. Run lengths identified in the previous row are combined with the current run length and amalgamated into the same feature or blob. The output of this module consists of single blob vectors, where each element consists of an identification (id) number and a set of run lengths. The biggest blob obtained is the wear region.

The blobs obtained provide a good delineation of the outer boundary; however, the blob interiors still contain dark pixels which must be filled prior to any feature measurement. A feature vector describing the perimeter of each blob is generated for each individual blob thereby allowing the interior dark pixels to be converted to bright pixels in order to obtain a homogeneous blob (i.e. without any interior dark valued pixels).

Finally, small area blobs that are present in the image must be eliminated, leaving only the tool wear blob. Morphological erosion, with a 5×5 structuring element, was performed on the binary image. The structuring element, an array consisting of 0's and 1's, defines a mask that can be used to control the direction of erosion. The 5×5 mask is laid on the object, such that the centre of the mask is on the edge of the object. When the 1's from the mask overlap the 1's in the image, the grey level at that pixel is set to zero. The image now contains a solitary feature from which the set of tool wear parameters can be calculated.

Tool wear parameters

Quantitative wear information can be extracted by deriving various classifiers from the binary image and then correlating them directly with the tool condition. A typical flank wear profile is divided into three regions (see Figure 6).

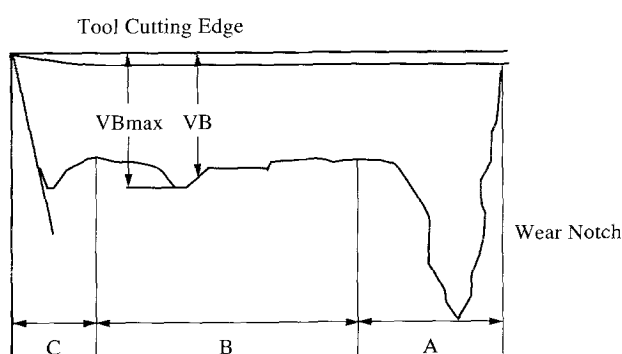


Fig. 6 Schematic diagram of a typical flank wear profile

- Zone A – Leading edge groove, which marks the outer end of the wear land.
- Zone B – A plateau consisting of uniform wear land.
- Zone C – Nose or trailing groove, which forms near the relief face and contributes significantly to surface roughness.

According to ISO (International Standards Organisation), tool life criteria are concerned only with the leading edge groove in zone A. In traditional tool condition monitoring, maximum wear land width is the most commonly used parameter to predict the extent of tool wear. If the profile is uniform, the tool can be used unless the average value of V_B is greater than 0.3 mm. For uneven wear, the maximum wear land width ($V_{B\max}$) should be less than 0.6 mm.

In this research, tool wear is characterized by deriving various morphological parameters from the wear profile. These parameters are classified into two groups:

Boundary descriptors

- (i) Maximum wear land width, $V_{B\max}$.

Regional descriptors

- (i) Area of the wear land; the number of pixels within the boundary of the wear region.
- (ii) Perimeter of the wear land; the length of the boundary in pixels.
- (iii) Compactness; a non-dimensional quantity, defined as (perimeter²/area).

Experimental results

Tool wear tests were conducted on a lathe, in the absence of a coolant. The wear growth patterns were observed on uncoated carbide tool inserts (grade VC 5), while turning hot rolled steel. The workpiece was turned for 15 minutes before the lathe was stopped. Then, the insert was positioned under the vision system and the flank wear images were recorded and stored in the computer. This procedure was repeated for every 10 min of cutting on the lathe until a total of seven cuts were performed using the same insert. The flank wear images recorded at different stages of the cutting

process are presented in Figs 7 and 8. The operating conditions for the cutting process (feed rate: 0.05 mm/rev, spindle speed: 550 rpm, depth of cut: 25 µin) were chosen such that the wear pattern is predominantly on the relief face (flank wear).

Figure 9(a) shows a plot of maximum wear land width versus cutting time. This plot reflects the traditional wear profile characteristic. In Fig. 9(a) the progression of the maximum wear land width toward the generally accepted criteria of a worn tool is evident. When this parameter reaches 0.5–0.6 mm range, a tool change should be initiated. The wear land perimeter and area are measured from the image in order to calculate the compactness (perimeter²/area). As shown in Fig. 9(b), the compactness curve has two distinct regions:

- An initial region showing a sharp decrease, due to the increase in wear region area for little corresponding increase in the wear notch depth.
- After about 55 min, the wear notch begins to grow rapidly giving an increase in perimeter for little additional increase in area of the wear region.

The results obtained from the vision system were compared with those obtained from a toolmaker's microscope. Maximum wear land width was the only parameter that was measured using the microscope and the values were found to be in close agreement.

The repeatability of the tool wear parameters was computed from five measurements of the tool wear profile obtained under the same illumination conditions. It can be estimated by:

$$R = t_{v,p}S \quad (4)$$

where $t_{v,p}$ is obtained from the Student-t distribution and S is the standard deviation (STD) given by:

$$S = \sqrt{\frac{\sum_{i=1}^N [(V(i) - \bar{V})^2]}{N - 1}} \quad (5)$$

where $\bar{V} = \left[\sum_{i=1}^N V(i) \right] / N$. The results of the repeatability test for flank wear measurements are presented in Table 2. It can be observed that there is little variation in the measured parameters.

Table 2 Repeatability of the measurement system

Trial #1	Maximum wear land width (mm)	Wear land area (mm ²)	Wear land perimeter (mm)
1	0.27	0.10	1.94
2	0.27	0.10	1.94
3	0.27	0.10	1.95
4	0.27	0.11	1.95
5	0.27	0.11	1.94
Mean	0.27	0.10	1.95
STD	0.00	0.01	0.01
$t_{v,p} \approx 8, P = 95$	2.31	2.31	2.31
Precision	0.004	0.01	0.01

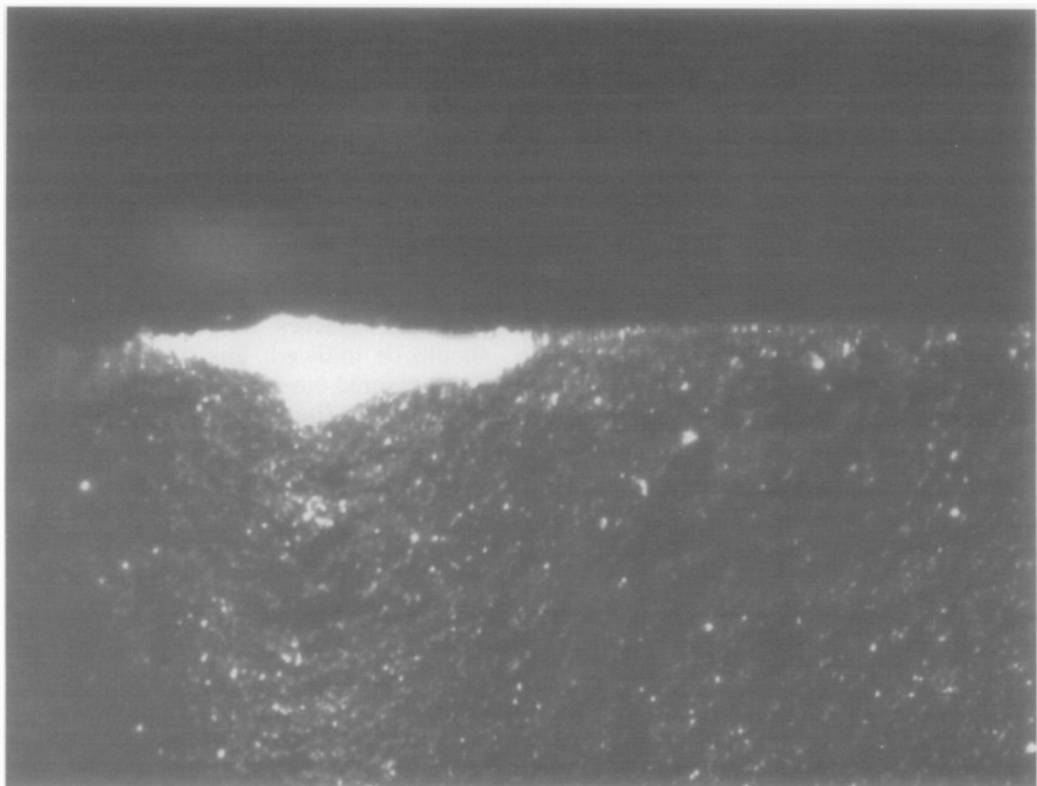


Fig. 7 Tool wear image obtained after machining for 25 min

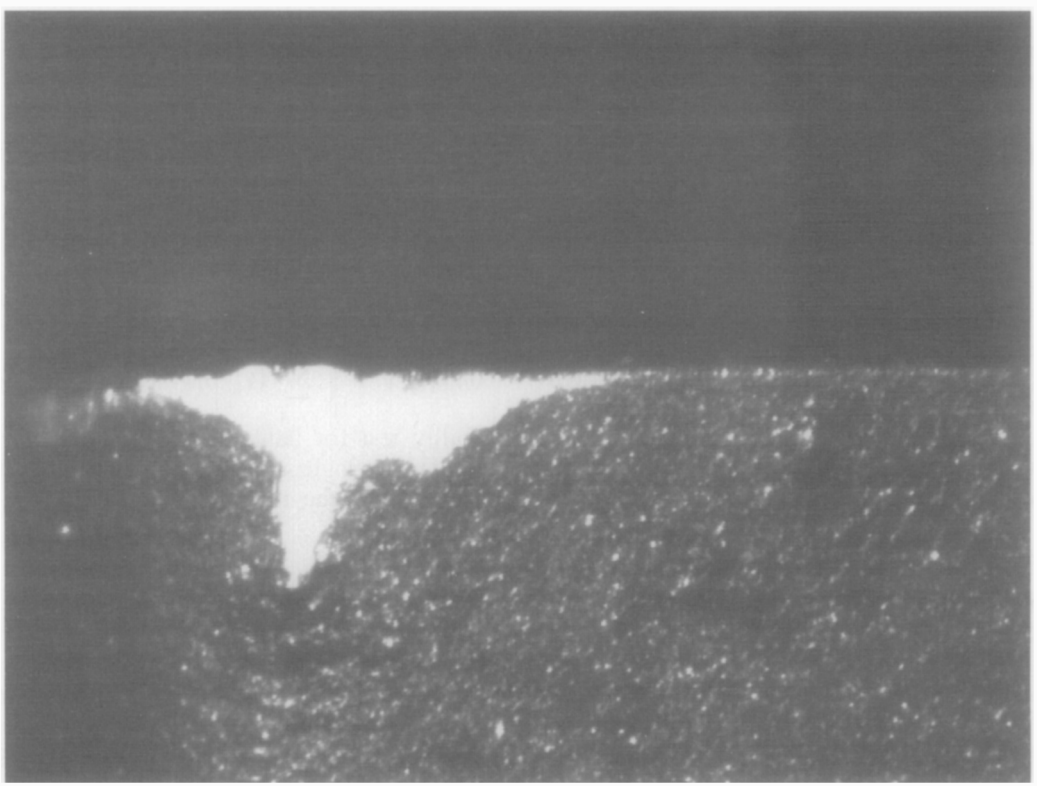


Fig. 8 Tool wear image obtained after machining for 45 min

Discussion

The research described in this paper has demonstrated a flank wear measurement technique employing a texture-based image segmentation algorithm. The use of texture

segmentation has improved processing of the tool wear images, compared to previous global thresholding techniques. The system presented is, therefore, relatively less susceptible to illumination variation caused by irregularities present on the tool surface. The developed

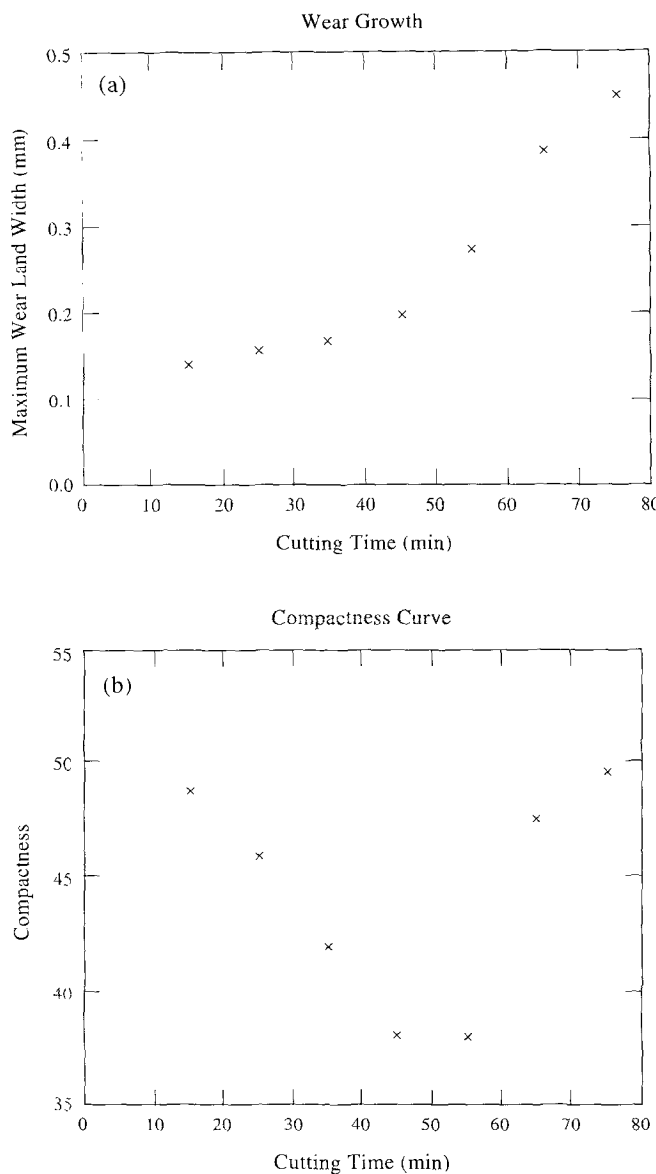


Fig. 9 (a) Maximum wear land width profile; (b) compactness curve

system can easily be extended for use in an unmanned environment, as it does not require any human interaction in the image processing phase.

Various morphological descriptors have been used to describe the wear growth with cutting time. From the wear land width plot, it can be observed that the wear progression is more rapid after a cutting time of 50 min. It was found that the compactness plot depicted the change in notch depth with respect to the rest of the profile quite effectively. The notch depth is an important wear indicator and, although compactness is not a recognized standard, the minimum point on the compactness plot does give a good indication of when the notch starts to grow rapidly. Additional research is being carried out to integrate the proposed vision-based flank wear monitor with an open architecture CNC machine tool controller. Therefore, it is proposed that compactness be used as an additional wear parameter

allowing machine tool control decisions to be based on two reliable indicators.

Further research will investigate the use of the vision system in measuring both tool wear and workpiece surface finish in a geometric adaptive control (GAC) configuration as proposed by Ulsoy and Koren¹⁸. Air-blown cleaning will also be investigated to remove any extraneous chips and dry up coolant on the tool.

Conclusions

A simple and inexpensive vision system has been implemented for flank wear monitoring during CNC turning. The processing scheme devised in this work is superior to previous methods, employing vision, due to the implementation of texture-based segmentation. Parameters, describing the characteristics of the wear profile, are used to describe the wear growth rate. Tool wear profiles obtained with the system are found to be similar to the traditional wear curves and the system's ability to measure tool wear parameters has been evaluated during repeatability and tool life tests. The new measurement system offers a convenient and non-contact method for the assessment of tool wear. The measurement procedure is fast and insensitive to vibration and ambient light variations.

References

- Boothroyd G. Fundamentals of Metal Machining and Machine Tools, McGraw-Hill, New York, 1975
- Thudy J. and Andrews G.C. A critical review of sensors for unmanned machining. *Ann. CIRP* 1983, **32**, 563-572
- Kurada S. and Bradley C. A vision system for in-cycle tool wear monitoring. *Proc. Eighth Int. Cong. Condition Monitoring and Diagnostic Engineering Management*, Kingston, Ontario, June 1995, Queen's University at Kingston, Ontario, Canada
- Chryssoolouris G. and Domroese M. Sensor integration for tool wear estimation in machining. *Proc. Symp. Sensors and Controls in Manufacturing*, ASME, New York, 1988, 115-123
- Konig W., Langhammer K. and Schemmel H.-U. Correlations between cutting force components and tool wear. *Ann. CIRP* 1972, **21**, 19-29
- Sihra T.S. The application of pattern recognition techniques for on-line monitoring of a milling process. *Proc. Eighth Int. Cong. Condition Monitoring and Diagnostic Engineering Management*, Kingston, Ontario, June 1995, Queen's University at Kingston, Ontario, Canada
- Jiang C.Y., Zhang Y.Z. and Xu H.J. In-process monitoring of tool wear stage by the frequency band-energy method. *Ann. CIRP* 1987, **36**, 45-48
- Rangwala S. and Dornfeld D.A. Integration of sensors via neural networks for detection of tool wear states. *Proc. Symp. Integrated and Intelligent Manufacturing Analysis and Synthesis*, ASME Winter Annual Meeting, New York, 1987, 109-120
- Du R., Elbestawi M.A. and Wu S.M. Automated monitoring of manufacturing processes Part 2: Applications. *J. Eng. Indust.* 1995, **117**, 133-142
- Weiss W., Lengeling A. and Huntrup V. Automatisierte Werkzeugüberwachung und-vermessung beim Fräsen mit Hilfe bildverarbeitender Systeme. *Technisches Messen* 1994, **61**, 473-476
- Lee Y.H., Bandyopadhyay P. and Kaminski B.D. Cutting tool wear measurement using computer vision. *Proc. Sensors '86 Conf.*, SME Technical Paper MR86-934, Detroit, MI, 1986
- Giusti F., Santochi M. and Tantussi G. On-line sensing of flank and crater wear of cutting tools. *Ann. CIRP* 1987, **36**, 41-44

13. **Pedersen K.B.** Wear measurement of cutting tools by computer vision. *Int. J. Mach. Tools Manuf.* 1990, **30**, 131–139
14. **Park J.J. and Ulsoy A.G.** On-line flank wear estimation using an adaptive observer and computer vision, Part 2: Experiment. *J. Eng. Indust.* 1993, **115**, 37–43
15. **Jeon J.U. and Kim S.W.** Optical flank wear monitoring of cutting tools by image processing. *Wear* 1988, **27**, 207–217
16. **Russ J.C.** The Image Processing Handbook, *CRC Press, Florida, USA*, 1992
17. **Russ, J.C.** Processing images with a local Hurst operator to reveal textural differences. *J. Comput. Assist. Microscopy* 1990, **2**, 249–257
18. **Ulsoy A.G. and Koren Y.** Control of machining processes. *J. Dyn. Syst. Meas. Control* 1993, **115**, 301–308